

Horsch Müller Jackson Eckelsbach Agarwal Vrabec Shchekin Hasse

The excess equimolar radius of liquid drops

Martin Horsch,* Erich A. Müller, and George Jackson†

*Department of Chemical Engineering and Chemical Technology,
Centre for Process Systems Engineering, Imperial College London, London SW7 2AZ, England*

Stefan Eckelsbach, Animesh Agarwal, and Jadran Vrabec

*Lehrstuhl für Thermodynamik und Energietechnik,
Institut für Verfahrenstechnik, Universität Paderborn,
Warburger Str. 100, 33098 Paderborn, Germany*

Alexander K. Shchekin

*Department of Statistical Physics, Faculty of Physics, St. Petersburg State University,
ul. Ulyanovskaya, Petrodvorets, 198504 St Peterburg, Russia*

Hans Hasse

*Lehrstuhl für Thermodynamik, Fachbereich Maschinenbau und Verfahrenstechnik,
Technische Universität Kaiserslautern, Erwin-Schrödinger-Str. 44, 67663 Kaiserslautern, Germany*

(Dated: 2nd December 2024)

The curvature dependence of the surface tension is related to the excess equimolar radius of liquid drops, i.e. the deviation of the equimolar radius from the capillarity approximation. Based on the Tolman approach and its interpretation by Nijmeijer *et al.* [J. Chem. Phys. **96**, 565 (1991)], the surface tension of spherical interfaces is analysed in terms of the pressure difference due to curvature. However, the excess equimolar radius, which can be obtained directly from the density profile, is used instead of the Tolman length here. Liquid drops of the truncated-shifted Lennard-Jones fluid are investigated by molecular dynamics simulation in the canonical ensemble, with equimolar radii ranging between 4 and 33 times the Lennard-Jones size parameter σ . In these simulations, the magnitude of the excess equimolar radius and the Tolman length is shown to be smaller than $\sigma/2$. Other methodical approaches, from which mutually contradicting claims have been deduced, are critically discussed, outlining possible sources of inaccuracy.

PACS numbers: 05.70.Np, 68.03.-g, 05.20.Jj, 68.03.Cd

I. INTRODUCTION

The capillarity approximation consists in neglecting the curvature dependence of the surface tension γ of a spherical liquid drop. Accordingly, the surface tension of a curved interface in equilibrium is approximated by the value γ_0 that is reached in the zero-curvature limit, i.e. for a planar vapour-liquid interface. The Young-Laplace equation [1, 2] for spherical interfaces relates it to a characteristic radius P of the liquid drop

$$\frac{\gamma_0}{P} = \frac{1}{2} (p' - p'') = \varphi, \quad (1)$$

called the capillarity radius here. Therein, both the factor $1/P$ and the difference between the liquid pressure p' and the vapour pressure p'' express the extent to which the surface is curved; the half pressure difference

$\varphi = (p' - p'')/2$ is introduced for convenience. Due to the equilibrium condition, the temperature is the same for both phases and the pressures p' and p'' correspond to the same chemical potential. The surface tension γ_0 of the planar phase boundary, which is relatively easy to access experimentally, couples these two measures of curvature as a proportionality constant.

In combination with an equation of state for the bulk fluid, microscopic properties such as the radius of a small liquid drop can thus be deduced from the macroscopic state of the surrounding vapour, i.e. from its supersaturation ratio, and vice versa. This approach is the most widespread interpretation of the Gibbs theory of interfaces [3, 4] and the point of departure for the classical nucleation theory (CNT) as introduced by M. Volmer and A. Weber [5] and further developed by Farkas [6] as well as subsequent authors [7–9]. The Gibbs approach presumes a sharp dividing surface between the phases, a conceptual image that does not reflect the physical phenomena present on the molecular length scale. However, this abstraction is precisely its strength. Instead of discussing thermodynamic properties such as the density, the pressure tensor and the free energy density in a localized way, excess quantities are assigned to the formal

* Co-affiliated with TU Kaiserslautern and Universität Paderborn

† Corresponding author: Prof. George Jackson, Imperial College London. Contact: +44 20 7594 5640; g.jackson@imperial.ac.uk; <http://www3.imperial.ac.uk/people/g.jackson>

dividing surface as a whole.

It should be noted that significant size effects on interface properties had already been detected experimentally by R. Weber [10] at the turn of the last century. This was also known to Farkas who stated explicitly that the capillarity approximation should be expected to fail for radii on the length scale of the intermolecular interactions [6]. In the absence of a better approximation, however, the surface tension of the planar phase boundary had to be used for nucleation theory, and little has changed in this respect in the meantime.

In case of significant deviations from the capillarity approximation, liquid drops cannot be characterized sufficiently by a single effective radius. Instead, the capillarity radius P is distinct from the equimolar radius Q , which is also known as the Gibbs adsorption radius. For a single-component system, the latter is defined by the zero excess density criterion

$$\int_0^Q dz z^2 [\rho(z) - \rho'(\mu, T)] + \int_Q^\infty dz z^2 [\rho(z) - \rho''(\mu, T)] = 0, \quad (2)$$

i.e. by comparing a step function based on the bulk liquid and vapour densities $\rho'(\mu, T)$ and $\rho''(\mu, T)$ as functions of the chemical potential μ and the temperature T , respectively, with the microscopic radial density profile $\rho(z)$. By convention, the density ρ expresses the number of particles per volume here, rather than their mass, and z denotes the distance from the centre of mass of the liquid drop. In the following discussion, T is treated as a parameter (instead of a variable), so that total differentials are to be understood as partial differentials at constant temperature.

For curved interfaces in equilibrium, the chemical potential deviates from its saturated value μ_s for a flat interface. In case of a drop, both phases are supersaturated. To realize this, it is sufficient to consider the Gibbs-Duhem equation for a curved phase boundary

$$d(p' - p'') = (\rho' - \rho'') d\mu. \quad (3)$$

For a planar interface, both phases coexist at saturation conditions ($\mu = \mu_s$) and the half pressure difference φ is zero. Raising p' over p'' therefore increases the chemical potential, which must be equal for both phases in equilibrium, so that its value exceeds μ_s . The precise conditions can be determined from the pressure difference between the fluid phases by means of an equation of state.

Beside P and Q , a thermodynamically relevant definition of the liquid drop size is given by the surface of tension radius

$$R = \frac{\gamma}{\varphi}, \quad (4)$$

which is also known as the Laplace radius. It is obtained by inserting the actual surface tension γ (not the planar

limit value) into the Young-Laplace equation. This radius can be related to the surface area a and to the volume V of the drop

$$R da = 2 dV. \quad (5)$$

The excess Landau free energy Σ of the surface thus evaluates to

$$R d\Sigma = 2\gamma dV, \quad (6)$$

in terms of the surface tension

$$\gamma = \frac{d\Sigma}{da}. \quad (7)$$

Modified versions of the Young-Laplace equation, which permit using different radii in an analogous way, were introduced by Buff [11, 12] and Kondo [13].

The present study deals with the deviation between the capillarity radius P , the equimolar radius Q and the surface of tension radius R of a liquid drop in equilibrium with a supersaturated vapour. As Tolman, following Gibbs, proved on the basis of axiomatic thermodynamics [14–16], one of these differences, the Tolman length

$$\delta = Q - R, \quad (8)$$

is sufficient to characterize the curvature dependence of the surface tension [16]

$$\frac{d \ln \gamma}{d \ln R} = 1 + \frac{1}{2} \left(\frac{\delta}{R} + \left[\frac{\delta}{R} \right]^2 + \frac{1}{3} \left[\frac{\delta}{R} \right]^3 \right)^{-1}. \quad (9)$$

It is important to point out that this equation is exact, strictly following the approach of Gibbs, i.e. without neglecting any higher-order terms. The cubic expression derives from an integral over the spherical density profile. However, Eq. (9) is often transformed into a polynomial expansion for γ_0/γ , which contains an infinite number of terms and has to be truncated, e.g. after the second-order contribution in terms of curvature [17]

$$\frac{\gamma_0}{\gamma} = 1 + \frac{2\delta_0}{R} + 2 \left(\frac{\ell}{R} \right)^2 + \mathcal{O}(R^{-3}). \quad (10)$$

Therein, δ_0 is the Tolman length in the zero-curvature (planar interface) limit. Castellanos *et al.* [18] conjectured that «the Tolman length is related to the interfacial width Δ^σ according to $\Delta^\sigma \approx 2\delta_0$.» The block length ℓ , which characterizes the effect of Gaussian curvature that becomes predominant when δ is very small or for systems where, due to an inherent symmetry, $\delta = 0$ holds by construction, was recently investigated by Block *et al.* [17]; a similar leading term, proportional to $R^{-2} \ln R$, was deduced by Bieker and Dietrich [19] from DFT based on a Barker-Henderson perturbation expression.

It should be kept in mind that the Tolman equation as given by Eq. (9) is valid for curved phase boundaries of

pure fluids in general, whereas truncated polynomial expansions in terms of $1/R$ like Eq. (10) necessarily break down for liquid drops on the molecular length scale. In practice, one of the major problems of the Tolman approach is that it analyses the surface tension in terms of the radii Q and R . While Q is immediately given by the density profile, R is by definition related to γ itself. Since for curved interfaces γ is disputed or unknown [20, 21], the surface of tension radius R is uncertain as well.

To resolve this issue, the present work reformulates Tolman's theory in terms of P and Q . This leads to an increase in clarity, since the capillarity radius P can be obtained on the basis of the surface tension in the planar limit γ_0 , which is experimentally accessible, and properties of the (stable and metastable) bulk fluid. It is related to the half pressure difference φ , which is a bulk property as well, since it can be determined from μ and T with an equation of state for the fluid. All information on the molecular structure of the curved interface is thus captured by a single undisputed quantity here, namely the equimolar radius Q .

For this approach, the excess equimolar radius, defined by

$$\eta = Q - P, \quad (11)$$

takes the place of the Tolman length, and the macroscopic quantity φ is used instead of $1/R$ as a measure of the curvature influence on the thermophysical properties of the interface and the bulk phases. In this way, the thermodynamics of liquid drops are discussed by following a new route that relies on density profiles and bulk properties only, avoiding the intricacies of defining the pressure tensor or the variation of the surface area as required by other approaches.

The present method is related to the «direct determination» of δ_0 proposed by Nijmeijer *et al.* [22] and recently applied by van Giessen and Blokhuis [23] on the basis of a diagram showing φQ as a function of $1/Q$ with

$$-\delta_0 = \frac{1}{\gamma_0} \left(\lim_{Q \rightarrow \infty} \frac{d}{d(1/Q)} \varphi Q \right), \quad (12)$$

as depicted in Fig. 1. However, the implementation suggested here is methodologically different from the van Giessen-Blokhuis approach which relies on a pressure tensor to obtain φ , whereas in the present work, the pressure difference is determined by molecular dynamics (MD) simulation of the bulk fluid. Applying the definitions of the capillarity radius and the excess equimolar radius, Eq. (12) transforms to

$$-\delta_0 = \lim_{Q \rightarrow \infty} \frac{d(Q/P)}{d(1/Q)} = \lim_{Q \rightarrow \infty} \frac{d(\eta/P)}{d(1/Q)}, \quad (13)$$

facilitating an analysis of interface properties in terms of the radii P and Q as well as the deviation η between them.

This article is structured as follows: Sec. II reviews the available routes to the Tolman length and the surface

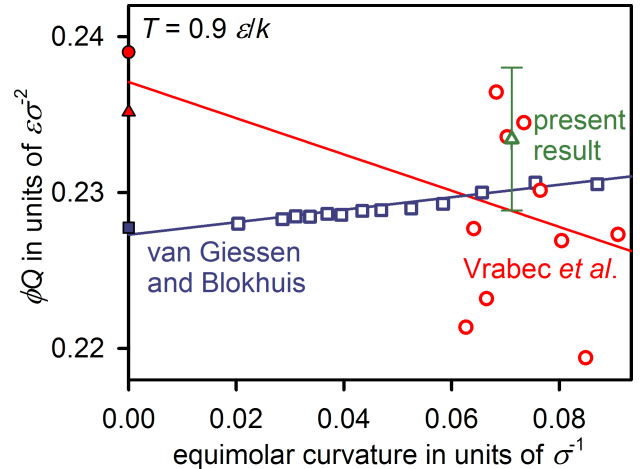


Figure 1. Diagram of van Giessen and Blokhuis [23], showing φQ over the equimolar curvature $1/Q$ for liquid drops of the truncated-shifted Lennard-Jones fluid at $T = 0.9 \varepsilon/k$, where the equimolar radius Q is determined from density profiles and φ from the difference between the values of the normal component of the Irving-Kirkwood pressure tensor in the homogeneous regions inside the liquid drop as well as outside, i.e. in the homogeneous supersaturated vapour. In comparison with the van Giessen-Blokhuis results (\square), the data of Vrabec *et al.* (\circ), which were obtained by the same method [24], are included here along with a present data point (\triangle) where φ was determined by MD simulation of the homogeneous fluid. The data for the planar surface tension γ_0 are taken from simulations of Vrabec *et al.* (\bullet) and van Giessen and Blokhuis (\blacksquare) as well as the correlation of Vrabec *et al.* (\blacktriangle). The solid lines are guides to the eye: In the planar limit, a positive slope corresponds to a negative Tolman length and vice versa, cf. Eq. (12).

tension by molecular simulation. MD simulation methods immediately related to nucleation itself, from which information on the excess free energy of curved interfaces can be deduced as well [25–27], are not included in this discussion; regarding that topic, the reader is referred to Chkonia *et al.* [28]. Sec. III briefly outlines how Tolman's thermodynamic approach is transformed by analysing the surface tension in terms of η and φ rather than δ and $1/R$. The methodology and the results of a series of canonical ensemble MD simulations, obtaining the excess equimolar radius on the basis of density profiles only, are presented in Sec. IV. An interpretation of these results is given in Sec. V, placing the present contribution in the context of the multitude of mutually contradicting hypotheses proposed in the literature.

II. THE TOLMAN LENGTH FROM MOLECULAR SIMULATION

A. Analysis of the planar interface

For the planar interface, the definition of the Tolman length by Eq. (8) ceases to be applicable, as the surface of tension radius R becomes ill-defined in the absence of a curvature, since the pressure is equal on both sides in this case. Therefore, the planar interface Tolman length δ_0 necessarily has to be derived from considerations pertaining to curved geometries. It can be obtained either by extrapolating results for δ to the limit $\varphi \rightarrow 0$ (i.e. $R \rightarrow \infty$) or by constructing the limit explicitly from expressions for the radii Q and R . The latter approach was followed by Fisher and Wortis [29] who, on the basis of Landau theory, derived the equation

$$-\delta_0 = \left(\int_{z=-\infty}^{z=\infty} d\rho_0(z) \frac{d\rho_0(z)}{dz} \right)^{-1} \int_{z=-\infty}^{z=\infty} d\rho_0(z) \frac{d\rho_0(z)}{d\ln z} + \frac{1}{\Delta\rho} \int_{z=-\infty}^{z=\infty} d\rho_0(z) z, \quad (14)$$

for the density profile $\rho_0(z)$ of the planar interface. This expression can also be extended to account for the pairwise density profile, whereby Eq. (14) becomes a limiting case [30, 31].

The available computational methods for evaluating the Tolman length of curved interfaces, however, involve the determination of the surface tension. It is usually the methodology related to this aspect that is both the crucial and the most debatable step, which is made evident by the contradictions between results for γ (and consequently for δ_0 as well) obtained from different methods. Three routes to the surface tension of liquid drops will now be discussed briefly: the virial route as implemented by Thompson *et al.* [32], the grand canonical route of Schrader *et al.* [33] and the variational route developed by Sampayo *et al.* [21].

Many different versions and combinations of these approaches exist [34, 35], but it would be vain to attempt a full appreciation of the whole spectrum here.

B. The virial route

The virial route to the surface tension is based on the Bakker-Buff equation for spherical interfaces [12, 32, 36, 37]

$$\gamma = R^{-2} \int_{z=0}^{z=\infty} dz z^2 [p_n(z) - p_t(z)], \quad (15)$$

in terms of the normal component $p_n(z)$ and the two (equal) tangential components $p_t(z)$ of the diagonalized pressure tensor, which is considered as a spherical average. This expresses the work required for a reversible isothermal deformation of the system that leads to an

infinitesimal increase of the surface at constant volume, which coincides with the associated free energy difference. It is sufficient to compute either the normal or the tangential pressure profile, since both are related by [32, 38]

$$\frac{dp_n}{d\ln z} = 2(p_t - p_n). \quad (16)$$

In mechanical equilibrium, Eq. (15) thus transforms to [32]

$$2\gamma^3 = -\varphi^2 \int_{z=0}^{z=\infty} dp_n(z) z^3, \quad (17)$$

a term in which R no longer appears. In this way, the surface of tension radius R can be obtained from the Young-Laplace equation once the surface tension γ is known.

The most widespread implementation of this approach in terms of intermolecular pair potentials is the Irving-Kirkwood (IK) pressure tensor [39], which was first applied to (spherical) interfaces by Buff [12] and underlies the simulation results of Vrabec *et al.* [24] as well as van Giessen and Blokhuis [23]. Its normal component is given by [32, 39]

$$p_n(z) = kT\rho(z) + \sum_{\{i,j\} \in \mathbf{S}} -\frac{du_{ij}}{dr_{ij}} \frac{|\mathbf{z} \cdot \mathbf{r}_{ij}|}{4\pi z^3 r_{ij}}, \quad (18)$$

wherein k is the Boltzmann constant and the summation covers the set \mathbf{S} containing all unordered pairs of particles i and j that are connected by a line intersecting a sphere of radius z around the centre of mass. The intersection coordinates relative to the centre of mass of the liquid drop are given by \mathbf{z} and the distance between the particles is expressed by \mathbf{r}_{ij} as well as $r_{ij} = |\mathbf{r}_{ij}|$, while $-du_{ij}/dr_{ij}$ is the force acting between the two particles i and j .

Regarding the virial route as described above, various issues arise:

- It is not clear to what extent the spherical average of the pressure tensor succeeds in accounting for the free energy contribution of capillary waves, i.e. the excited vibrational modi of the interface [40, 41].
- Irving and Kirkwood [39] originally proposed their expression for the special case of «a single component, single phase system». Its derivation relies on truncating an expansion in terms of derivatives of the pairwise density $\rho^{(2)}$ after the first term, thereby disregarding the density gradient completely. For a liquid drop, this can lead to inaccuracies: «at a boundary or interface ... neglecting terms beyond the first may not be justified» [39].
- By construction, the virial route cannot be separated from the assumption of a mechanical equilibrium that underlies both the basic approach, i.e. Eqs. (15) to (16), and the derivation of the IK

pressure tensor, cf. Eq. (18). For nanoscopic liquid drops, however, configurations deviating from the equilibrium shape correspond to a significant fraction of the partition function.

The Harasima pressure tensor [37], where the set \mathbf{S} is defined differently and the tangential pressure profile $p_t(z)$ is computed instead of $p_n(z)$, has been found to agree rather well with the IK tensor [24, 35, 42], which is hardly surprising since both methods rely on the same basic approach.

C. The grand canonical route

From an analysis of the canonical partition function and its dependence on the characteristic length L of otherwise similar systems, Binder [41] derived scaling laws concerning the probability $\omega(\rho_{\min})$ for a relatively small subvolume to have the density ρ_{\min} related to a maximum of the local free energy, i.e. the least probable local density between ρ' and ρ'' . It follows that «the probability of a *homogeneous* state with order parameter ρ_{\min} decreases exponentially fast with the volume» while those cases where the corresponding subvolume is situated within a phase boundary have a probability which «decreases exponentially fast with the interface area» [41]. The surface excess of the Landau free energy (per surface area) can thus be determined as

$$f^E = \lim_{a \rightarrow \infty} \frac{\Sigma}{a} = kT \lim_{L \rightarrow \infty} \frac{\ln \omega(\rho_{\min})}{a(L)}, \quad (19)$$

which is related to the surface tension by $\gamma = d\Sigma/da$. Therein, the term $a(L)$ describes the dependence of the surface area on the characteristic length of the system [41], e.g. $a(L) = 2L^2$ for a planar slab in a cubic volume $V = L^3$ with a periodic boundary condition.

Small subvolumes of a canonical system in the thermodynamic limit ($N \rightarrow \infty$) are equivalent to systems with constant μ , V and T so that grand canonical Monte Carlo (GCMC) simulation can be applied. Umbrella sampling may be used to fully sample the relevant range of values for the order parameter [43, 44], corresponding to the number of particles N present in the grand canonical system. Thereby, a profile is obtained for the free energy density $f(N)$ or $f(\rho)$, i.e. the Landau free energy per volume unit, in dependence of the order parameter.

To analyse liquid drops of a certain size, however, the limit $a \rightarrow \infty$ cannot be applied since the area a of the surface of tension is fixed. Instead, the excess term $f^E(Q)$ is determined from expressions based on the equimolar radius [33]

$$f(\rho) = \frac{V'}{V} \rho'(Q) \mu_Q + \frac{V''}{V} \rho''(Q) \mu_Q + \frac{4\pi Q^2}{V} f^E(Q). \quad (20)$$

$V' = 4\pi Q^3/3$ is the volume associated with the liquid phase here, $V'' = V - V'$ is the remainder of the volume

and $\rho'(Q)$ as well as $\rho''(Q)$ are bulk densities related to the liquid drop and the surrounding vapour. The chemical potential μ_Q is equal for the vapour and liquid phases, but different from both the saturated bulk value μ_s and the chemical potential μ used for the grand canonical simulation itself. This formalism has recently been employed by Schrader *et al.* [20, 33] as well as Block *et al.* [17], leading to mutually consistent results.

While the original method of Binder [41] is beyond reproach, the following points concerning the spherical geometry should be kept in mind:

- Following the approach of Schrader *et al.* [33], the surface tension γ can be accessed only indirectly, e.g. from Eq. (6), based on the surface of tension radius R which also has to be obtained indirectly. Thereby, care should be taken not to confuse f^E with γ , or Q with R .
- Since the infinite size limit, cf. Eq. (19), does not apply to nanoscopic liquid drops and the systems under consideration can be extremely small, it is not generally possible to neglect the contribution of homogeneous configurations to $f(\rho)$ [41].
- Assuming $4\pi Q^2$ to be the surface area associated with the excess Landau free energy of the system, as in Eq. (20), is actually tantamount to applying the capillarity approximation. Such an approach may be justified under certain circumstances, but for investigating the *deviation* from capillarity it is of limited use only.

Other umbrella sampling based methods [45, 46], which will not be discussed here in detail, are confronted with similar difficulties, in particular regarding the relation between the surface tension and the excess free energy of the surface.

D. The variational route

The variational route to the surface tension is based on Bennett's general considerations regarding molecular simulation of free energies and entropic quantites [47]. In the canonical ensemble, the free energy difference $\Delta A = A_1 - A_0$ between two states with equal N , V and T is given by the quotient of the respective canonical partition functions Z_0 and Z_1 , which evaluates to an expression in terms of internal energy differences [47]

$$\exp\left(\frac{\Delta A}{kT}\right) = \frac{Z_0}{Z_1} = \frac{\langle \min(1, \exp([E_1 - E_0]/[kT])) \rangle_1}{\langle \min(1, \exp([E_0 - E_1]/[kT])) \rangle_0}, \quad (21)$$

where the index of the angular brackets denotes the system for which an ensemble average is taken. Bennett proposed to obtain these energy differences from «separately-generated samples» [47] for E_0 and E_1 . If

the two systems differ in the size of a phase boundary, then the free energy difference can be related to the surface tension, assuming that all other deviations between the two states are accurately taken into account.

Gloor *et al.* [34] introduced a version of this approach where differences between the two states are obtained from a single simulation run for an unperturbed system with the partition function Z_0 . Corresponding configurations of the second, perturbed system are generated by small affine transformations, keeping the volume and the number of particles in both phases constant. In the limit of an infinitesimal distortion of the volume, Eq. (21) simplifies to [34, 48]

$$\frac{\Delta A}{kT} = - \left\langle \exp \left(\frac{E_0 - E_1}{kT} \right) \right\rangle_0, \quad (22)$$

as the ensemble densities of the unperturbed and perturbed systems converge, so that a separate averaging is no longer required. A third-order expansion [48]

$$\begin{aligned} \frac{\Delta A}{kT} = & \frac{\langle \Delta E \rangle}{kT} - \frac{\langle \Delta E^2 \rangle - \langle \Delta E \rangle^2}{2(kT)^2} \\ & + \frac{\langle \Delta E^3 \rangle - 3 \langle \Delta E^2 \rangle \langle \Delta E \rangle + 2 \langle \Delta E \rangle^3}{6(kT)^3}, \end{aligned} \quad (23)$$

based on a Gaussian fit, can be used to increase the precision of the simulation results [21, 34]. The surface tension is then immediately given by $\Delta A/\Delta a$, since the distortion of the interface itself (as opposed to its increase in area) has no contribution to the free energy difference [14].

In analogy with the Widom test particle method [49], this implementation of the variational route is also called the test area method [34, 50]. Following Sampayo *et al.* [21], it can be applied to curved interfaces, where the affine transformation scales one of the cartesian axes by the factor $1/(1+\xi)$ and the remaining ones by $(1+\xi)^{1/2}$. For $\xi > 0$, this creates an oblate shape and the area of the surface of tension is increased by [51]

$$\frac{\Delta a}{\pi Q^2} = 2(1+\xi) + \frac{\ln([1+\Xi]/[1-\Xi])}{(1+\xi)^2 \Xi} + \mathcal{O}\left(\frac{\delta \Delta a}{Q^3}\right), \quad (24)$$

with the ellipticity of the average equimolar surface in the perturbed system given by $\Xi = [1 - (1+\xi)^{-3}]^{1/2}$. In the prolate case ($\xi < 0$), the corresponding term is $\Xi = [1 - (1-\xi)^{-3}]^{1/2}$ with [51]

$$\frac{\Delta a}{\pi Q^2} = 2 \left(\frac{\arcsin \Xi}{\Xi(1-\xi)^{1/2}} - \xi - 1 \right) + \mathcal{O}\left(\frac{\delta \Delta a}{Q^3}\right). \quad (25)$$

It can be shown that the first-order term in Eq. (23) is equivalent to the Kirkwood-Buff [52] virial route expression for the surface tension [53]. The higher-order terms therefore presumably capture the deviation between the virial and variational routes due to fluctuations or, equivalently, the contribution of non-equilibrium configurations to γ . Thus, the higher-order contribution to Eq.

(23) may be related to the closed expression derived by Percus *et al.* [54] for the deviation between the actual free energy and an approximation based on the local pressure.

From this point of view, the following aspects of the method merit further consideration:

- While finite differences of higher order are taken into account for the energy, no such terms are considered for the surface area here. Clearly, the variance of ΔE is partly caused by the variance of Δa . For instance, if a liquid drop is already non-spherical in a configuration of the unperturbed system, test deformations can move it towards its equilibrium shape, intuitively decreasing its surface area. The use of Q for defining the surface area, cf. Eqs. (24) and (25), may lead to further deviations.
- The variance of ΔE accounts for surface oscillations such as capillary waves, which directly relate to equilibrium properties of the interface and therefore do not depend on the statistical mechanical ensemble. However, it can also be influenced by fluctuations regarding ρ' (at constant V') or V' (at constant ρ'). These modi are ensemble dependent, since they are coupled to the density of the vapour phase. Canonically, their amplitude increases with the total volume and is ill-defined in the thermodynamic limit $V \rightarrow \infty$. Therefore, the surface tension from the variational route may depend on the constraints imposed on the system by the ensemble.
- Although the volume associated with each of the phases is invariant for test area transformations, there is still a distortion with respect to the equilibrium conformation. The method is therefore limited to isotropic phases, since shearing an anisotropic phase could induce a contribution to ΔA from the bulk as well.

III. DEVIATION OF THE EQUIMOLAR RADIUS FROM CAPILLARITY

From the Tolman equation in its approximate polynomial form, cf. Eq. (10), the excess equimolar radius η can be related to the Tolman length δ by

$$\eta = (\delta + R) - P = \delta + \frac{\gamma}{\varphi} \left(1 - \frac{\gamma_0}{\gamma} \right) = -\delta + \mathcal{O}(R^{-1}), \quad (26)$$

so that its magnitude in the zero-curvature limit is obtained as

$$-\delta_0 = \eta_0, \quad (27)$$

which is essentially equivalent to Eq. (13).

Both in the planar limit and in the presence of curvature effects, it is therefore possible to express the Tolman approach in terms of the easily accessible quantities η and φ , rather than δ and $1/R$. The point of departure for this is the exact closed form of the Tolman

equation, cf. Eq. (9). As it should be recalled, this expression is derived from the Gibbs-Duhem equation, the Young-Laplace equation and the Gibbs adsorption equation [16]; hence, it is fully based on axiomatic thermodynamics. As opposed to truncated power series like Eq. (10), it remains valid when the radius R becomes similar or smaller in magnitude than the Tolman length. Polynomial expansions in terms of δ/R necessarily fail to capture this limit.

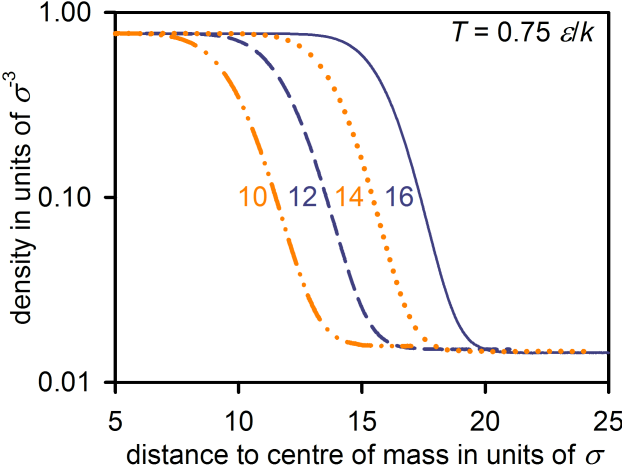


Figure 2. Density profiles from canonical MD simulations of LJTS liquid drops at $T = 0.75 \varepsilon/k$ with equimolar radii of $Q = 9.977 \pm 0.001$ (—), 12.029 ± 0.003 (—), $13.974 \pm 0.002 \sigma$ (···) and $15.967 \pm 0.001 \sigma$ (—), cf. Tabs. I and II.

From the Young-Laplace equation, it follows that

$$\frac{dR}{d\varphi} = \frac{d\gamma}{\varphi d\varphi} - \frac{\gamma}{\varphi^2}, \quad (28)$$

while the reduced length scale appearing in the Tolman equation

$$\frac{\delta}{R} = \frac{\eta\varphi + \gamma_0}{\gamma} - 1, \quad (29)$$

is transformed using Eqs. (1), (4), (8) and (11). The Tolman equation can thus be converted to

$$\frac{d\gamma}{d\varphi} = -\frac{2\gamma}{\varphi} \left(\frac{\delta}{R} + \left[\frac{\delta}{R} \right]^2 + \frac{1}{3} \left[\frac{\delta}{R} \right]^3 \right) \quad (30)$$

$$= \frac{2\gamma}{3\varphi} \left(1 - \left[\frac{\eta\varphi + \gamma_0}{\gamma} \right]^3 \right). \quad (31)$$

This equation is fully equivalent to Eq. (9).

For $\varphi \rightarrow 0$, further considerations are required. There, the curvature dependence of γ as specified by Eq. (31) is only self-consistent under an additional condition. To prove this, it is helpful to consider the exact Tolman equation in a different form

$$\frac{d\gamma}{d\varphi} = \frac{2}{\gamma^2} \left(\frac{1}{3} [F - \eta^3 \varphi^2] - \gamma_0 \eta [\gamma_0 + \eta\varphi] \right), \quad (32)$$

which follows from Eq. (31) by expanding the cubic term. Therein, F is defined by

$$F = \frac{\gamma^3 - \gamma_0^3}{\varphi}. \quad (33)$$

For the sake of brevity, the notation $q_i = \lim_{\varphi \rightarrow 0} d^i q / d\varphi^i$ is used here for the i -th derivative of a quantity q in the zero-curvature limit. The slope of γ can be obtained by inserting

$$F_0 = (\gamma^3)_1 = 3\gamma_0^2 \gamma_1, \quad (34)$$

into Eq. (32), which yields

$$\gamma_1 = 2\eta_0. \quad (35)$$

Expanding the excess equimolar radius as

$$\eta = \eta_0 + \eta_1 \varphi + \mathcal{O}(\varphi^2), \quad (36)$$

and inserting this expression as well as Eq. (35) into the planar limit for Eq. (32) leads to

$$(\gamma^3)_2 = 12\gamma_0 \eta_0^2, \quad (37)$$

and

$$\gamma_0 \gamma_2 = -4\eta_0^2. \quad (38)$$

It is by considering the zero-curvature limit for the third derivative of γ^3 that a theorem for the slope of η can now be deduced. Based on Eqs. (34) and (37), a Taylor expansion for $d(\gamma^3)/d\varphi$ in terms of φ

$$\frac{d}{d\varphi} \gamma^3 = (\gamma^3)_1 + (\gamma^3)_2 \varphi + \frac{1}{2} (\gamma^3)_3 \varphi^2 + \mathcal{O}(\varphi^3), \quad (39)$$

yields

$$\begin{aligned} F &= \frac{1}{\varphi} \int_0^\varphi d\varphi \left(\frac{d}{d\varphi} \gamma^3 \right) \\ &= 6\gamma_0^2 \eta_0 + 6\gamma_0 \eta_0^2 \varphi + \frac{\varphi^2}{6} (\gamma^3)_3 + \mathcal{O}(\varphi^3). \end{aligned} \quad (40)$$

From Eqs. (35) to (40)

$$6\gamma_0 (\gamma_0 \eta_1 + \eta_0^2) + \frac{\varphi}{6} (\gamma^3)_3 = 0 + \mathcal{O}(\varphi), \quad (41)$$

follows by applying the full Tolman equation, cf. Eq. (32), in the planar limit. However, this implies

$$\eta_1 = -\frac{\eta_0^2}{\gamma_0}, \quad (42)$$

which constitutes a necessary boundary condition for the Tolman approach in terms of η and φ .

Thus, while there is a direct correspondence between δ_0 and η_0 , no such relation exists in case of δ_1 and η_1 , i.e. the respective derivatives (in terms of φ) in the zero-curvature limit; instead, η_1 is fully determined by η_0 and

thus by δ_0 , the Tolman length of the planar interface. This means that data on the excess equimolar radius for large radii have a double significance regarding the planar limit: on the one hand, they can be extrapolated to $\varphi = 0$, leading to an estimate for the planar Tolman length and the curvature dependence of γ to first order in terms of φ or $1/R$; on the other hand, the slope of η is relevant itself, since its zero-curvature limit η_1 also provides information on η_0 .

The equivalent of the exact Tolman equation in terms of the excess equimolar radius η and the half pressure difference φ is Eq. (31). An expansion as a power series, analogous to Eq. (10), is given by

$$\gamma = \gamma_0 + 2\eta_0\varphi - \frac{2\eta_0^2}{\gamma_0}\varphi^2 + \mathcal{O}(\varphi^3). \quad (43)$$

The planar limit, where higher order terms can be neglected, can be treated accurately by expressions like Eq. (43). Away from the planar limit, Eq. (31) applies without any further condition (since the boundary condition for the slope of η is relevant for $\varphi \rightarrow 0$ only), whereas Eq. (43) becomes an approximation.

IV. THE EXCESS EQUIMOLAR RADIUS FROM MOLECULAR SIMULATION

With the *mardyn* MD program, developed by Bernreuther and co-workers [55–57], the canonical ensemble was simulated for small systems, corresponding to equilibrium conditions for nanoscopic liquid drops surrounded by supersaturated vapours. The truncated-

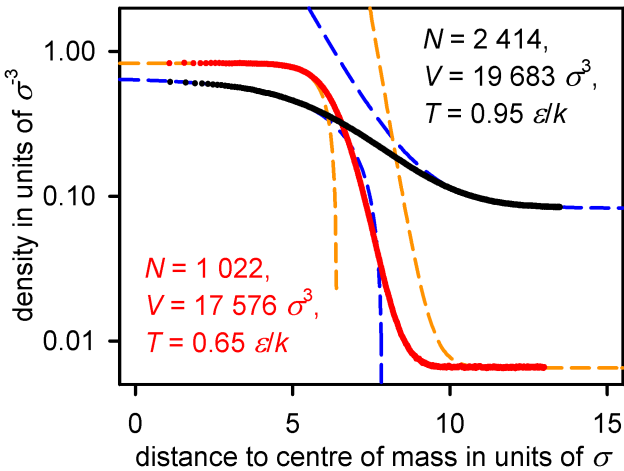


Figure 3. Density profiles from canonical MD simulations of LJTS liquid drops at $T = 0.65$ and $0.95 \varepsilon/k$, showing the average densities from simulation (\bullet) and exponential approximants ($--$). The steeper profile corresponds to the lower temperature.

shifted Lennard-Jones (LJTS) pair potential

$$u(r) = \begin{cases} 4\varepsilon \left[\sigma^6(r_c^{-6} - r^{-6}) + \sigma^{12}(r^{-12} - r_c^{-12}) \right], & \text{for } r < r_c, \\ 0, & \text{for } r \geq r_c, \end{cases} \quad (44)$$

with the size parameter σ , the energy parameter ε and a cutoff radius of $r_c = 2.5 \sigma$ was applied as a fluid model. This potential is a prototypical model for the bulk fluid properties of simple spherical conformal fluids (e.g. noble gases and methane), cf. Vrabec *et al.* [24]. On account of this, numerous studies on nanoscopic liquid drops have been published [17, 23, 24, 58–62]. The LJTS fluid can thus be regarded as the main benchmark for theoretical and simulation approaches to the problem of curved vapour-liquid interfaces.

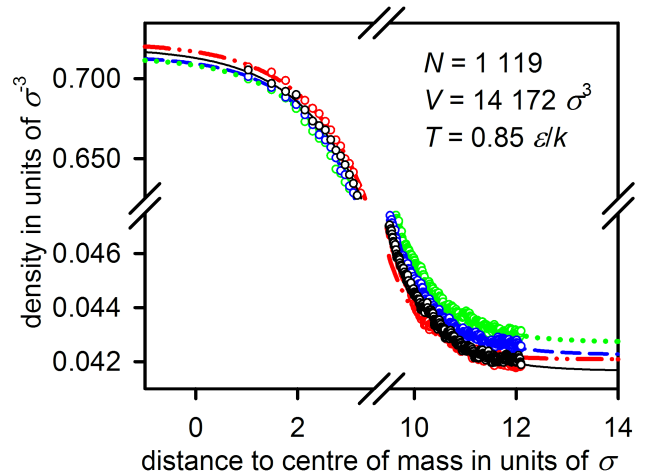


Figure 4. Density profiles from a single canonical MD simulation of a LJTS liquid drop at $T = 0.85 \varepsilon/k$, showing the average densities from simulation (\circ) and exponential approximants (lines) corresponding to the sampling intervals $2\ 000 - 3\ 000$ (\cdots ; green), $3\ 000 - 4\ 000$ ($\cdots - \cdots$; red), $4\ 000 - 5\ 000$ ($--$; blue) and $5\ 000 - 6\ 000$ time units ($-$; black) after simulation onset. The standard deviation between the densities at an infinite distance from the interface, according to the exponential fits for all sampling intervals of a single MD simulation, was used to determine the error of the bulk densities here.

Certain general properties of this simple model, taking only short-range interactions into account, can be assumed to carry over to polar fluids as well [63], except for temperatures in the vicinity of the critical point. It is clear, however, that a qualitatively different behaviour should be expected for liquid drops formed by water with and without ions [64, 65], liquid crystals [66] and similar complex organic molecules. Such systems are beyond the scope of this study.

Liquid drops were investigated at temperatures between $T = 0.65$ and $0.95 \varepsilon/k$, covering most of the range between the triple point temperature, which is approximately $0.55 \varepsilon/k$ according to Bolhuis and Chandler

[67], $0.618 \varepsilon/k$ as determined by Toxværd [68] and $0.65 \varepsilon/k$ according to van Meel *et al.* [60], and the critical temperature which several independent studies have consistently obtained as $1.08 \varepsilon/k$ for the LJTS fluid [24, 69, 70]. The Verlet leapfrog algorithm was employed for solving the classical equations of motion numerically with an integration time step of 0.002 in Lennard-Jones time units, i.e. in $\sigma\sqrt{m/\varepsilon}$, where m is the mass of a particle. Cubic simulation volumes with 290 to 126 000 particles, applying the periodic boundary condition, were equilibrated for at least 2 000 time units. Subsequently, spherically averaged density profiles $\rho(z)$, with their origin ($z = 0$) at the centre of mass of the whole system, were constructed with a binning scheme based on equivoluminal concentric spheres using sampling intervals between 1 000 and 40 000 time units, depending on the (expected) total simulation time, to gather multiple samples for each system. Figures 2 to 4 provide examples of the density profiles obtained according to this method.

The density profiles of LJTS vapour-liquid interfaces are known to agree well with an expression based on two hyperbolic tangent terms, to which $\rho(z)$ has been successfully correlated for liquid drops by Vrabec *et al.* [24]. The present method, however, merely requires the bulk densities ρ' and ρ'' corresponding to a certain value of μ or φ , which were determined here by correlating the outer part of the density profile and extrapolating it to regions far from the interface. The densities of the co-existing fluid phases were thus deduced from simulation results by adjusting the exponential terms

$$\begin{aligned}\rho' &= \rho(z) + \alpha' \exp(\beta'[z - z']), \\ \rho'' &= \rho(z) - \alpha'' \exp(\beta''[z'' - z]),\end{aligned}\quad (45)$$

to the data for the inner- and outermost spherical bins of the density profiles, cf. Fig. 3. These terms, which are based on those employed by Lekner and Henderson [53], asymptotically agree with the hyperbolic tangent expression of Vrabec *et al.* [24]. From the liquid and vapour densities ρ' and ρ'' of the fit to Eq. (45), the equimolar radius Q was calculated according to Eq. (2). The respective margins of error were obtained as standard deviations from the profiles belonging to different sampling intervals of the same MD simulation, cf. Fig. 4, of which there were at least three in all cases. The corresponding pressures p' and p'' were computed by canonical MD simulation of the bulk fluid at the respective densities.

For the surface tension in the zero-curvature limit, the values $\gamma_0(0.65 \varepsilon/k) = 0.680 \pm 0.009$, $\gamma_0(0.75 \varepsilon/k) = 0.493 \pm 0.008$, $\gamma_0(0.85 \varepsilon/k) = 0.317 \pm 0.007$ and $\gamma_0(0.95 \varepsilon/k) = 0.158 \pm 0.006 \varepsilon\sigma^{-2}$ were taken from the correlation of Vrabec *et al.* [24]; the error corresponds to the individual data points for γ_0 from the same source. In case of $T = 0.9 \varepsilon/k$, the higher precision of the computations of van Giessen and Blokhuis [23] was exploited, using the value $\gamma_0 = 0.227 \pm 0.002 \varepsilon\sigma^{-2}$ obtained from a linear fit to data for the curved interface [23], cf. Fig. 1. The assumption made for the error is rather generous in this case, considering the even higher confidence suggested by

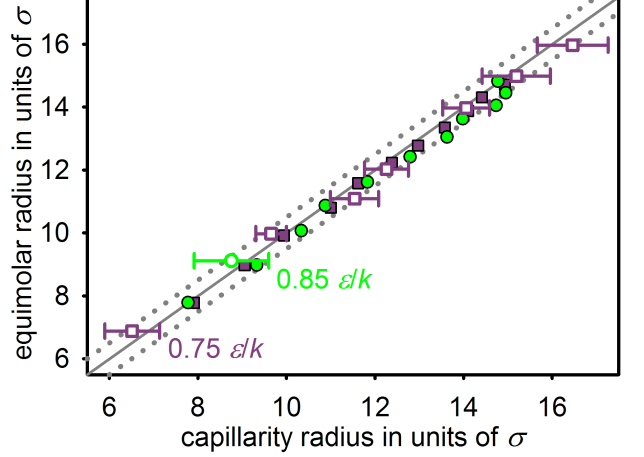


Figure 5. Equimolar radius Q over capillarity radius P for LJTS liquid drops, from density profiles and bulk pressures determined by the present canonical MD simulations at $T = 0.75$ (□) and $0.85 \varepsilon/k$ (○), in comparison with results from previous work of Vrabec *et al.* [24] at $T = 0.75$ (■) and $0.85 \varepsilon/k$ (●), using pressure differences based on evaluating the IK tensor in the approximately homogeneous regions inside and outside the liquid drop. The solid diagonal line is defined by $Q = P$ and thus by an excess equimolar radius of $\eta = 0$, while the dotted lines correspond to $\eta = \pm 0.5 \sigma$.

the agreement between the individual data points for φQ .

Combining these quantities leads to the capillarity radius P and the excess equimolar radius η . Note that the margin of error for η , as indicated in Tab. I, contains contributions quantifying the accuracy of γ_0 and the precision of the MD simulations of the liquid drop itself as well as the homogeneous vapour and liquid phases. While the vapour pressure p'' and the equimolar radius Q could be obtained with a high precision, the liquid pressure and the surface tension in the zero-curvature limit are major sources of uncertainty here. In both cases, methodical changes can be expected to increase the precision significantly: regarding γ_0 , it can be seen from Fig. 1 that it is possible today to reach a level of confidence beyond that of the data from Vrabec *et al.* [24] which were used here. For p' , approaches based on the chemical potential, which can be determined in any region of the simulation volume (including the vapour phase), can be expected to lead to significant improvements in combination with a reliable equation of state or high-precision simulations of the grand canonical ensemble.

A full list of the simulation results where η could be determined with error bars smaller than 1σ is given in Tab. II. Note that to achieve full consistency with the Tolman approach, the bulk densities ρ' and ρ'' from Eq. (45) have to match those of the bulk fluid at the same temperature and chemical potential as the two-phase system. Regarding liquid drops with $Q > 8 \sigma$, this is certainly the case, since constant density regions coexisting with the interface are actually present, cf. Fig. 2. The values determined for the smallest drops here, however, rely on the

Table I. Error discussion for the excess equimolar radius η of LJTS liquid drops at the temperature $T = 0.75 \varepsilon/k$. The number of particles N , the volume V of the periodic simulation box and the total simulation time t for the simulations of the liquid drops are indicated alongside the contributions to the uncertainty of η from the pressure p' of the liquid phase (determined by canonical MD simulation of the bulk liquid), the surface tension γ_0 of the planar vapour-liquid interface, cf. Vrabec et al. [24], the vapour pressure p'' (analogous to p') and the equimolar radius Q (from the density profiles of the liquid drops). Note that the time unit, i.e. $\sigma\sqrt{m/\varepsilon}$, corresponds to 500 simulation time steps here. The flat symbols (\flat) indicate the fraction of the margin of error for η due to the respective quantities. All values are given in Lennard-Jones units, and the error in terms of the last digit is specified in parentheses. In the subsequent discussion, the cases where the uncertainty of η exceeds 1 σ are disregarded.

N	$V [\sigma^{-3}]$	$t [\sigma\sqrt{m/\varepsilon}]$	$p' [\varepsilon\sigma^{-3}]$	$\flat p'$	$\flat \gamma_0$	$p'' [\varepsilon\sigma^{-3}]$	$\flat p''$	$Q [\sigma]$	$\flat Q$	$\eta [\sigma]$
497	10 648	60 000	0.6(1)	84 %	5.9 %	0.0135(3)	0.23 %	4.33(5)	9.5 %	2.5(5)
1 418	21 952	48 176	0.16(1)	82 %	17 %	0.01136(5)	0.37 %	6.883(3)	0.5 %	0.4(6)
1 766	21 952	6 000	0.14(3)	94 %	5.3 %	0.0110(2)	0.58 %	7.61(1)	0.55 %	0(2)
3 762	39 304	221 244	0.113(2)	53 %	45 %	0.01042(4)	1 %	9.977(1)	0.28 %	0.3(3)
5 161	54 872	64 219	0.096(3)	63 %	34 %	0.0104(1)	2.4 %	11.089(4)	0.82 %	-0.4(5)
6 619	74 088	162 678	0.090(2)	59 %	40 %	0.01007(2)	0.75 %	12.029(3)	0.57 %	-0.2(5)
10 241	110 592	185 460	0.080(1)	56 %	43 %	0.00985(2)	0.58 %	13.974(2)	0.29 %	-0.1(5)
12 651	140 608	32 594	0.075(2)	66 %	32 %	0.00974(4)	1.2 %	14.981(6)	0.78 %	-0.2(8)
15 237	166 375	135 348	0.070(2)	66 %	33 %	0.00969(1)	0.35 %	15.967(1)	0.15 %	-0.5(8)
17 113	169 418	6 006	0.08(1)	89 %	9.8 %	0.00969(9)	0.78 %	16.689(4)	0.18 %	2(2)
24 886	238 328	27 272	0.069(9)	90 %	9.7 %	0.00947(3)	0.3 %	18.969(5)	0.17 %	2(3)
28 327	238 328	6 006	0.056(9)	92 %	7.5 %	0.00945(3)	0.28 %	19.950(8)	0.18 %	-1(5)
38 753	247 673	6 000	0.050(7)	90 %	8.8 %	0.00932(5)	0.69 %	22.391(7)	0.15 %	-2(4)
125 552	697 078	6 006	0.042(5)	89 %	9.6 %	0.00908(9)	1.6 %	33.31(1)	0.21 %	3(5)

Table II. Number of particles N , volume V of the periodic simulation box and temperature T of the present canonical ensemble MD simulations of the LJTS fluid and equilibrium properties of the liquid drop as well as the surrounding vapour, i.e. the respective densities ρ' , ρ'' and pressures p' , p'' as well as the capillarity radius P , the equimolar radius Q and the excess equimolar radius η . For radii above 8 σ , these values can be reliably regarded as identical with those corresponding to the present theoretical approach, which is highlighted by a bold typeface. In case of smaller radii (oblique typeface), inaccuracies could arise due to the application of exponential approximants, cf. Fig. 3 and Eq. (45), so that the respective values can, at present, be acknowledged as phenomenological quantities only. All values are given in Lennard-Jones units, and the error in terms of the last digit is specified in parentheses.

N	$V [\sigma^3]$	$T [\varepsilon/k]$	$\rho' [\sigma^{-3}]$	$\rho'' [\sigma^{-3}]$	$p' [\varepsilon\sigma^{-3}]$	$p'' [\varepsilon\sigma^{-3}]$	$P [\sigma]$	$Q [\sigma]$	$\eta [\sigma]$
291	8 999	0.65	0.857(5)	0.0090(2)	0.65(8)	0.0054(1)	2.1(3)	3.90(1)	1.8(3)
1 022	17 576	0.65	0.830(1)	0.00651(7)	0.22(2)	0.00397(4)	6.3(6)	6.407(2)	0.1(6)
497	10 648	0.75	0.81(1)	0.0214(6)	0.6(1)	0.0135(4)	1.8(5)	4.33(5)	2.5(5)
1 418	21 952	0.75	0.777(1)	0.0173(1)	0.16(1)	0.01136(5)	6.5(6)	6.883(3)	0.4(6)
3 762	39 304	0.75	0.7721(2)	0.01566(6)	0.113(2)	0.01042(4)	9.7(4)	9.977(1)	0.3(4)
5 161	54 872	0.75	0.7703(2)	0.0156(2)	0.096(3)	0.0104(1)	11.5(5)	11.089(4)	-0.5(6)
6 619	74 088	0.75	0.7697(2)	0.01506(4)	0.091(2)	0.01007(2)	12.3(5)	12.029(3)	-0.2(5)
10 241	110 592	0.75	0.7685(1)	0.01469(3)	0.080(2)	0.00985(2)	14.1(5)	13.974(2)	-0.1(5)
12 651	140 608	0.75	0.7679(2)	0.01451(7)	0.075(2)	0.00974(4)	15.2(8)	14.981(6)	-0.2(8)
15 237	166 375	0.75	0.7673(2)	0.01442(2)	0.070(2)	0.00969(1)	16.5(8)	15.967(1)	-0.5(8)
1 119	14 172	0.85	0.733(7)	0.0421(5)	0.23(5)	0.0273(2)	3.1(9)	6.79(6)	2.5(9)
3 357	32 768	0.85	0.7135(8)	0.0371(5)	0.097(5)	0.0249(2)	8.8(8)	9.11(1)	0.4(9)
2 031	21 952	0.9	0.687(3)	0.0573(8)	0.13(1)	0.0369(3)	5.1(8)	6.79(6)	1.7(9)
4 273	29 791	0.9	0.6773(9)	0.0532(2)	0.082(4)	0.03516(7)	9.7(9)	10.086(9)	0.4(9)
11 548	85 184	0.9	0.6738(1)	0.0504(2)	0.0672(6)	0.03396(8)	13.7(4)	14.054(8)	0.4(4)
2 414	19 683	0.95	0.662(2)	0.0825(2)	0.169(7)	0.05032(8)	2.7(3)	6.86(3)	4.2(3)

validity of the Eq. (45) fit and can be considered valid only as far as this expression itself does not introduce any major deviations, an assertion that remains open to further examination; a version of the present method computing p' via μ could resolve this issue as well.

V. DISCUSSION

Previous authors have made qualitatively contradicting claims on the magnitude of the Tolman length as well as its sign: Tolman himself expected δ to be positive and smaller than the length scale of the dispersive interaction, a conjecture that Kirkwood and Buff [52] affirmed from a statistical mechanical point of view, based on a virial approach. Subsequent studies, however, have also found δ to be equal to zero [19, 58], positive and large [24, 61], i.e. $\delta > \sigma$, negative and small [21, 23, 71], i.e. $-\sigma < \delta < 0$, or negative and diverging in the planar limit [72], i.e. $\delta_0 = -\infty$, while others have claimed that the sign of δ is curvature dependent itself [73, 74]. Thereby, they have only proven the mutual inconsistency of their assumptions and methods, while nothing is truly known about δ and the dependence of the surface tension on curvature.

The new approach introduced in Sec. III is strictly based on axiomatic thermodynamics and relies on the fact that $\delta_0 = -\eta_0$ holds in the planar limit. From the values for η displayed in bold face in Tab. II, corresponding to $Q > 8 \sigma$, the excess equimolar radius for liquid drops of the LJTS fluid is unequivocally shown to be smaller in magnitude than $\sigma/2$, while its remains unclear whether it is positive, negative, of both signs (depending on curvature) or equal to zero. Since this means that on the present level of accuracy, no significant dependence of γ on the radius of the liquid drop could be detected, the statement of Mareschal *et al.* [75] regarding cylindrical interfaces applies here as well: considering «the large fluctuations in the bulk liquid phase», cf. the error discussion in Tab. I, «we tentatively conclude that the surface tension is independent of the curvature of the liquid-vapor interface or else that this dependence is very weak.»

The only view that can be definitely dismissed is that of a large and positive Tolman length, previously held by some of the present authors on the basis of results from

the virial route to the surface tension, employing the IK pressure tensor [24, 61]. As Fig. 5 shows, the previous simulation results are actually consistent with those from the present study if they are interpreted in terms of the radii P and Q . Thereby, following the approach of van Giessen and Blokhuis [23], only the density profile and the pressure in the homogeneous region inside and outside the liquid drop are taken into account, whereas the normal pressure along the interface is not considered at all. Since the deviation between present and previous data disappears in such a representation, the disagreement must be caused by a breakdown of the virial route as implemented by Thompson *et al.* [32]. Possible sources of error for this approach were outlined above. Nonetheless, more detailed methodological investigations are expedient to determine which approximations are actually responsible for major inaccuracies, and whether they can be corrected or the virial route to the surface tension has to be discarded altogether.

ACKNOWLEDGMENTS

The present work contributes to the IMEMO project of the German Federal Ministry of Education and Research (BMBF). It was conducted under the auspices of the Boltzmann-Zuse Society of Computational Molecular Engineering (BZS). The position of M. T. Horsch at the Imperial College London was funded by a fellowship within the postdoc programme of the German Academic Exchange Service (DAAD), and the computations were performed on the NEC Nehalem cluster *laki* at the High Performance Computing Center Stuttgart (HLRS) with resources allocated according to the grant MMHBF. At the HLRS, the authors would like to thank M. F. Bernreuther for his support in general and for co-ordinating the MMHBF grant as well as the development of the MD code *mardyn*. Furthermore, D. Reguera López and J. Wedekind (Barcelona), F. Römer (London), M. Schrader (Mainz), Z. Lin, S. K. Miroshnichenko, S. Olma, Z. Wei (Paderborn) and D. V. Tatyanenko (St. Petersburg) as well as S. Dietrich, S. Grottel, C. Niethammer and G. Reina (Stuttgart) are acknowledged for contributing to various theoretical and practical issues through helpful suggestions and their participation in relevant discussions or by assisting at the debugging process.

[1] T. Young, Phil. Trans. R. Soc. Lond. **95**, 65 (1805).
 [2] P.-S. de Laplace, *Traité de méchanique céleste*, vol. 3 (Bachelier, Paris, 1806).
 [3] J. W. Gibbs, Transact. Connecticut Acad. Arts Sci. **3**, 108 (1878).
 [4] J. W. Gibbs, Am. J. Sci. (ser. 3) **16**, 441 (1878).
 [5] M. Volmer and A. Weber, Z. phys. Chem. **119**, 277 (1926).
 [6] L. Farkas, Z. phys. Chem. **125**, 236 (1927).
 [7] R. Becker and W. Döring, Ann. Phys. **24**, 719 (1935).
 [8] F. Kuhrt, Z. Phys. **131**, 185 (1952).
 [9] J. Feder, K. C. Russell, J. Lothe and G. M. Pound, Adv. Phys. **15**, 111 (1966).
 [10] R. H. Weber, Ann. Phys. **4**, 706 (1901).
 [11] F. P. Buff, J. Chem. Phys. **19**, 1591 (1951).
 [12] F. P. Buff, J. Chem. Phys. **23**, 419 (1955).
 [13] S. Kondo, J. Chem. Phys. **25**, 662 (1956).
 [14] R. C. Tolman, J. Chem. Phys. **16**, 758 (1948).

[15] R. C. Tolman, *J. Chem. Phys.* **17**, 118 (1949).

[16] R. C. Tolman, *J. Chem. Phys.* **17**, 333 (1949).

[17] B. J. Block, S. K. Das, M. Oettel, P. Virnau and K. Binder, *J. Chem. Phys.* **133**, 154702 (2010).

[18] A. J. Castellanos Suárez, J. Toro Mendoza and M. García Sucre, *J. Phys. Chem. B* **133**, 5981 (2009).

[19] T. Bieker and S. Dietrich, *Physica A* **252**, 85 (1998), *Physica A* **259**, 466 (1998).

[20] M. Schrader, P. Virnau, D. Winter, T. Zykova-Timan and K. Binder, *Eur. Phys. J. Spec. Top.* **177**, 103 (2009).

[21] J. G. Sampayo, A. Malijevský jr., E. A. Müller, E. de Miguel and G. Jackson, *J. Chem. Phys.* **132**, 141101 (2010).

[22] M. J. P. Nijmeijer, C. Bruin, A. B. van Woerkom, A. F. Bakker and J. M. J. van Leeuwen, *J. Chem. Phys.* **96**, 565 (1991).

[23] A. E. van Giessen and E. M. Blokhuis, *J. Chem. Phys.* **131**, 164705 (2009).

[24] J. Vrabec, G. K. Kedia, G. Fuchs and H. Hasse, *Mol. Phys.* **104**, 1509 (2006).

[25] H. Matsubara, T. Koishi, T. Ebisuzaki and K. Yasuoka, *J. Chem. Phys.* **127**, 214507 (2007).

[26] J. Vrabec, M. Horsch and H. Hasse, *J. Heat Transfer* **131**, 043202 (2009).

[27] Z.-Y. Hou, L.-X. Liu, R.-S. Liu, Z.-A. Tian and J.-G. Wang, *Chem. Phys. Lett.* **491**, 172 (2010).

[28] G. Chkonia, J. Wölk, R. Strey, J. Wedekind and D. Reguera, *J. Chem. Phys.* **130**, 064505 (2009).

[29] M. P. A. Fisher and M. Wortis, *Phys. Rev. B* **29**, 6252 (1984).

[30] E. M. Blokhuis and D. Bedeaux, *Mol. Phys.* **80**, 705 (1993).

[31] T. V. Bykov and A. K. Shchekin, *Inorganic Materials* **35**, 641 (1999).

[32] S. M. Thompson, K. E. Gubbins, J. P. R. B. Walton, R. A. R. Chantry and J. S. Rowlinson, *J. Chem. Phys.* **81**, 530 (1984).

[33] M. Schrader, P. Virnau and K. Binder, *Phys. Rev. E* **79**, 061104 (2009).

[34] G. J. Gloor, G. Jackson, F. J. Blas and E. de Miguel, *J. Chem. Phys.* **123**, 134703 (2005).

[35] A. Ghoufi, F. Goujon, V. Lachet and P. Malfreyt, *Phys. Rev. E* **77**, 031601 (2008).

[36] G. Bakker, *Kapillarität und Oberflächenspannung*, no. 6 in *Handbuch der Experimentalphysik* (Akademische Verlagsgesellschaft, Leipzig, 1928).

[37] A. Harasima, *J. Phys. Soc. Jpn.* **8**, 343 (1953).

[38] V. G. Baidakov and G. S. Boltachev, *Phys. Rev. E* **59**, 469 (1999).

[39] J. H. Irving and J. G. Kirkwood, *J. Chem. Phys.* **18**, 817 (1950).

[40] J. R. Henderson and J. Lekner, *Mol. Phys.* **36**, 781 (1978).

[41] K. Binder, *Phys. Rev. A* **25**, 1699 (1982).

[42] J. P. R. B. Walton, D. J. Tildesley, J. S. Rowlinson and J. R. Henderson, *Mol. Phys.* **48**, 1357 (1983).

[43] G. M. Torrie and J. P. Valleau, *J. Comp. Phys.* **23**, 187 (1977).

[44] P. Virnau and M. Müller, *J. Chem. Phys.* **120**, 10925 (2004).

[45] M. J. McGrath, J. N. Ghogomu, N. T. Tsona, J. I. Siepmann, B. Chen, I. Napari and H. Vehkämäki, *J. Chem. Phys.* **133**, 084106 (2010).

[46] R. B. Nellas, S. J. Keasler, J. I. Siepmann and B. Chen, *J. Chem. Phys.* **132**, 164517 (2010).

[47] C. H. Bennett, *J. Comp. Phys.* **22**, 245 (1976).

[48] R. W. Zwanzig, *J. Chem. Phys.* **22**, 1420 (1954).

[49] B. Widom, *J. Chem. Phys.* **39**, 2808 (1963).

[50] F. J. Blas, L. G. MacDowell, E. de Miguel and G. Jackson, *J. Chem. Phys.* **129**, 144703 (2008).

[51] J. G. Sampayo Hernández, Ph.D. thesis (2010), Imperial College London.

[52] J. G. Kirkwood and F. P. Buff, *J. Chem. Phys.* **17**, 338 (1949).

[53] J. Lekner and J. R. Henderson, *Mol. Phys.* **34**, 333 (1977).

[54] J. K. Percus, L. A. Pozhar and K. E. Gubbins, *Phys. Rev. E* **51**, 261 (1995).

[55] M. Bernreuther and J. Vrabec, in *High Performance Computing on Vector Systems*, edited by M. Resch, T. Bönisch, K. Benkert, T. Furui and W. Bez (Springer, Heidelberg, 2006), pp. 187–195, ISBN 3-540-29124-5.

[56] M. Bernreuther, C. Niethammer, M. Horsch, J. Vrabec, S. Deublein, H. Hasse and M. Buchholz, *Innovatives Supercomputing in Deutschland* **7**, 50 (2009).

[57] M. Buchholz, H.-J. Bungartz and J. Vrabec, *Journal of Computational Science* (2010), submitted.

[58] Y. A. Lei, T. Bykov, S. Yoo and X. C. Zeng, *J. Am. Chem. Soc.* **127**, 15346 (2005).

[59] R. Holyst and M. Litniewski, *Phys. Rev. Lett.* **100**, 055701 (2008).

[60] J. A. van Meel, A. J. Page, R. P. Sear and D. Frenkel, *J. Chem. Phys.* **129**, 204505 (2008).

[61] M. Horsch, J. Vrabec and H. Hasse, *Phys. Rev. E* **78**, 011603 (2008).

[62] I. Napari, J. Julin and H. Vehkämäki, *J. Chem. Phys.* **133**, 154503 (2010).

[63] I. Nezbeda, *Mol. Phys.* **103**, 59 (2005).

[64] R. G. Harrison and M. H. P. Ambaum, *Proc. Roy. Soc. A* **464**, 2561 (2008).

[65] N. Galamba, *J. Chem. Phys.* **133**, 124510 (2010).

[66] M. Houssa, L. F. Rull and J. M. Romero Enrique, *J. Chem. Phys.* **130**, 154504 (2009).

[67] P. G. Bolhuis and D. Chandler, *J. Chem. Phys.* **113**, 8154 (2000).

[68] S. Toxværd, *J. Phys. Chem. C* **111**, 15620 (2007).

[69] W. Shi and J. K. Johnson, *Fluid Phase Equilib.* **187–188**, 171 (2001).

[70] B. Smit, *J. Chem. Phys.* **96**, 8639 (2002).

[71] S. J. Hemingway, J. R. Henderson and J. S. Rowlinson, *Faraday Symp. Chem. Soc.* **16**, 33 (1981).

[72] P. Bryk, R. Roth, K. R. Mecke and S. Dietrich, *Phys. Rev. E* **68**, 031602 (2003).

[73] K. Koga, X. C. Zeng and A. K. Shchekin, *J. Chem. Phys.* **109**, 4063 (1998).

[74] J. Julin, I. Napari, J. Merikanto and H. Vehkämäki, *J. Chem. Phys.* **133**, 044704 (2010).

[75] M. Mareschal, M. Baus and R. Lovett, *J. Chem. Phys.* **106**, 645 (1997).